

Measurements of Charge Transfer Inefficiency in a CCD With High-Speed Column Parallel Readout

André Sopczak, *Member, IEEE*, Khaled Bekhouche, Chris Damerell, Tim Greenshaw, Michal Koziel, Konstantin Stefanov, Tuomo Tikkanen, Tim Woolliscroft, and Steve Worm

Abstract—Charge Coupled Devices (CCDs) have been successfully used in several high energy physics experiments over the past two decades. Their high spatial resolution and thin sensitive layers make them an excellent tool for studying short-lived particles. The Linear Collider Flavour Identification (LCFI) collaboration is developing Column-Parallel CCDs (CPCCDs) for the vertex detector of a future Linear Collider. The CPCCDs can be read out many times faster than standard CCDs, significantly increasing their operating speed. A test stand for measuring the charge transfer inefficiency (CTI) of a prototype CPCCD has been set up. Studies of the CTI have been performed at a range of readout frequencies and operating temperatures.

Index Terms—Charge traps, data analysis, detectors, particle detectors, particle tracking, radiation damage, radiation effects in devices, semiconductor device radiation effects, signal analysis.

I. INTRODUCTION

THE study of radiation hardness is crucial for the application of CCD detectors in High Energy Physics experiments [1]–[4]. The LCFI collaboration has been developing and testing new CCD detectors for about 10 years [1]–[5]. Previous experimental results on CCD radiation hardness were reported for example in [6]–[10]. Several models increased the understanding of radiation damage effects in CCDs [11]–[13]. The measurements and analyses reported in this paper have been carried out in the LCFI collaboration [3]. Simulation and modeling of CCD radiation hardness effects for a CCD prototype with sequential readout was reported at IEEE'2005 [14]; comparing full TCAD simulations with analytic models was reported at IEEE'2006 [15] and in [16]; simulation and modeling of a CCD prototype with column parallel readout (CPCCD) was reported at IEEE'2007 [17] and in [18].

This work focuses on experimental measurements and a method to determine the charge transfer inefficiency (CTI) performed with the CPCCD at a test stand at Liverpool University.

Manuscript received November 15, 2008; revised March 19, 2009, and May 29, 2009. Current version published October 07, 2009. Presented on behalf of the LCFI Collaboration.

A. Sopczak, K. Bekhouche, and M. Koziel are with Lancaster University, Lancaster, U.K. (e-mail: andre.sopczak@cern.ch; khaledbekhouche@yahoo.com; michal.koziel@cern.ch).

C. Damerell, K. Stefanov, and S. Worm are with the STFC Rutherford Appleton Laboratory, Rutherford, U.K. (e-mail: c.damerell@rl.ac.uk; k.d.stefanov@rl.ac.uk; steven.worm@cern.ch).

T. Greenshaw and T. Woolliscroft are with Liverpool University, Liverpool, U.K. (e-mail: green@liv.ac.uk; woolliscroft@gmail.com).

T. Tikkanen is with Liverpool University, Liverpool, U.K., and also with Leicester University, Leicester, U.K. (e-mail: tvt1@star.le.ac.uk).

Color versions of one or more of the figures in this paper are available online at <http://ieeexplore.ieee.org>.

Digital Object Identifier 10.1109/TNS.2009.2026648

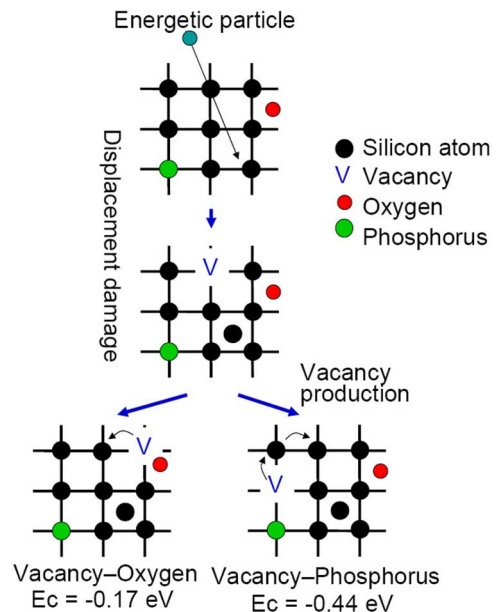


Fig. 1. Schematic view of how radiation damage is created in phosphorus-doped silicon. Two main types of vacancy defect are created: Vacancy-Oxygen (electron trap at 0.17 eV below the conduction band) and Vacancy-Phosphorus (electron trap at 0.44 eV below the conduction band).

The environment with high radiation near the interaction point at a future Linear Collider creates damage to the CCD material which leads to defects acting as electron traps in the silicon, as indicated in Fig. 1. The radiation level at a Linear Collider is estimated to be 5×10^{11} e/cm² per year and 10^{10} n/cm² per year at the inner vertex detector layer (14 mm radius) [16], [19], [20]. The mechanism of creating traps has been discussed in the literature, for example in [21]–[23]. These traps result in charge transfer inefficiency. In a phosphorus-doped device, two main types of traps are created. The first one is relatively shallow with energy level 0.17 eV below the conduction band and the second is deep with energy level 0.44 eV below the conduction band.

The column parallel technology is in development to cope with the required readout rate. CPC1 is a two-phase CCD prototype capable of 50 MHz readout frequency. In this paper we demonstrate the method to determine the CTI value with an un-irradiated CPCCD (CPC1).

II. TEST STAND FOR CCD OPERATION AND CRYOSTAT UNIT

A test stand has been set up with readout electronics and a cryostat unit. The temperature range of the cryostat is from room temperature down to about -140 °C. This temperature has been achieved with cold nitrogen gas by boiling liquid nitrogen. The

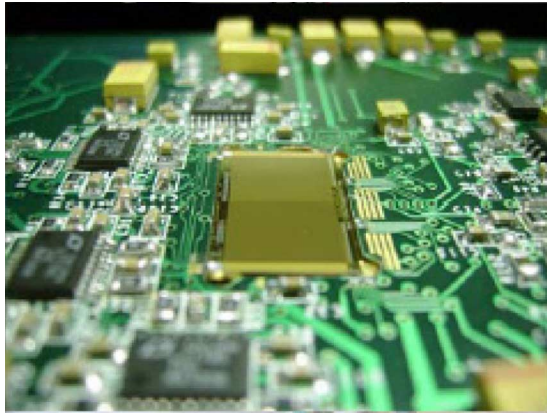


Fig. 2. CPC1 (in the center of the picture) with external electronics.

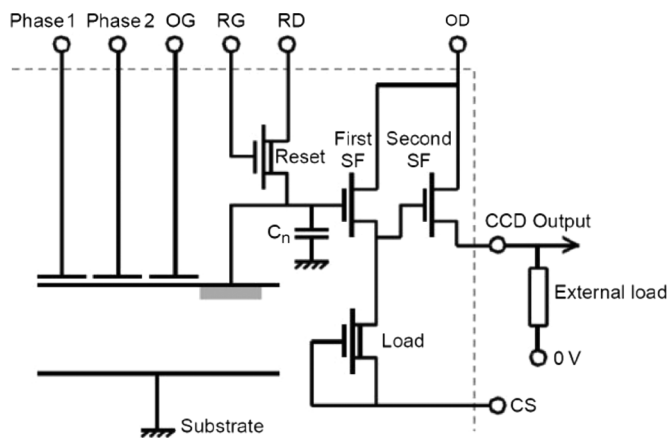


Fig. 3. On-chip amplifier with a floating diffusion detection node.

very low operating temperature is required to obtain sensitivity to the CTI peak structure for 0.17 eV traps where the peak position is expected to be near $-130\text{ }^{\circ}\text{C}$ [18]. This is for particular clocking conditions used in the setup. The CPC1 is a 2-phase CCD with $400(\text{V}) \times 750(\text{H})$ pixels, $20 \times 20\ \mu\text{m}^2$ size each pixel. Initial measurements have been performed on an un-irradiated device in standalone mode, where the signals from four columns of the CCD were amplified and connected to external 14-bit ADCs. A ^{55}Fe source emitting 6 keV X-rays was attached to a holder at a distance of 5 cm from the CCD to provide the signal charge. Fig. 2 shows a picture of CPC1 and the associated control and front-end readout electronics, which were also placed in the cryostat, wherefrom the four outputs were fed to rack-mounted amplifiers and ADCs.

Fig. 3 illustrates the on-chip amplifier. The main purpose of the on-chip amplifier in a CCD is the conversion of a charge packet into a voltage or a current. The change in the detection node voltage ($V = Q/C_n$) when a charge packet enters the node is sensed by the on-chip amplifier. In order to achieve a large bandwidth a two-stage source follower amplifier is used. The first stage (First SF) consists of a source follower and a current sink for biasing purposes. The second stage (Second SF) drives the external load. The reset FET, controlled by RG, is connected to the floating diffusion region. In the off-state it can collect the next charge packet and in the on-state it resets the

detection node to a reference voltage (RD). The bias voltage CS determines the bias current of the first stage.

The schematic diagram in Fig. 4 illustrates the electronics used to drive and read out the CPCCD. The apparatus is controlled by a LabView program through interface crates. The sequencer receives the master clock from the signal generator to provide a clock for the ADC and Sine Module and to trigger a pulse generator, which produces the reset signal “RG” for the CCD output gate. The sine module produces two clock signals for the two-phase CCD. In addition, an AC signal for output gate “OG” is generated.

It was observed that the CTI increased sharply when the amplitude of the sinusoidal clock pulses applied to read out the CCD was reduced to less than 2 V peak-to-peak. In order to suppress any effect from the clock amplitude, settings for each data acquisition were tuned to produce $3.00\ \text{V}_{\text{pp}}$ clock pulses. The timing settings (delays) depend on the readout frequency and operating temperature and had to be adjusted for each measurement. The performance of the drivers limited the maximum clocking frequency to about 22 MHz. The X-ray hit rate (occupancy) is kept constant. We expect that the errors on the CTI calculation decrease when increasing the occupancy. If we consider that 10 points are sufficient to fit the X-ray peak with a Gaussian function, the occupancy would be $10/5000 = 0.2\%$, where 5000 is the number of frames (4×400 pixels). In these measurements the occupancy was small (about 0.1%), resulting from the rather low activity of the ^{55}Fe source. Such a low occupancy is expected in Linear Collider operations, and has also been used in recent simulations [18]. Our cryostat did not allow placing the source very far from the detector. This may have caused some non-uniformity in the irradiation across the CCD. This non-uniformity is estimated to be about a 1% reduction at the edges of the sensitive area compared to the center.

Our method is based on the typical methods used for serially read out CCDs [24], [25], where CTI is determined by fitting a line to the read out charge signal as function of read (pixel) number, which is equal to the number of charge transfers needed to transfer the charge collected in that pixel across the CCD into the readout electrode. A linear function can be expected when the CTI is small.

III. SIGNAL MEASUREMENT AND REMOVING CHARGE SHARING BY USING A 3×3 CLUSTER METHOD

The fast ADCs convert the signal charge after amplification with a wideband preamplifier. The four columns are read out in 4 channels by ADCs. Three columns (channels 1 to 3) are adjacent whereas channel 4 is separate. The signal charges of 4×400 pixels plus 4×10 overclocks were acquired in 3000–5000 frames per measurement. This leads to a sufficient statistical precision (around few times 10^{-5}). The collected data have been analysed using the ROOT package [26]. First, we begin by applying correlated double sampling, where the difference between the signals of two consecutive pixels is taken to be the signal charge collected by the latter pixel. This decreases electronic noise. Common mode noise is reduced with the help of the overclocks, which are charges read out

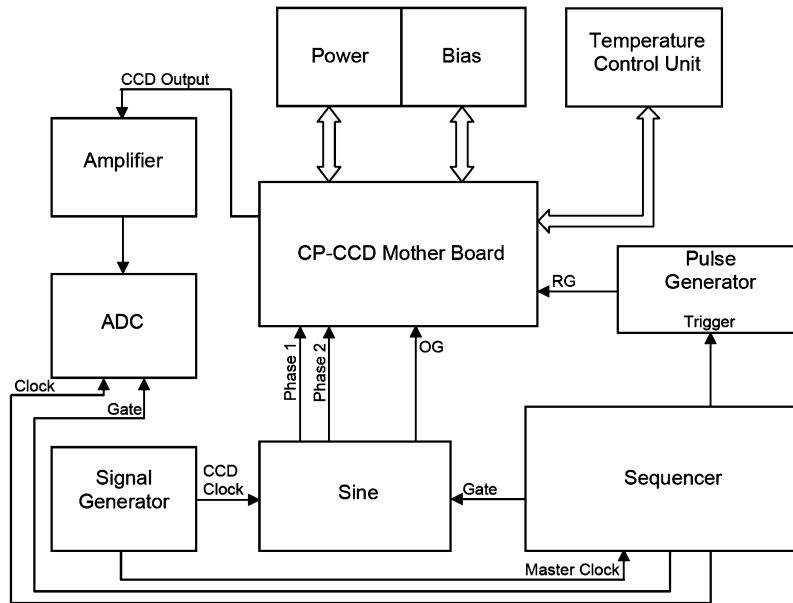


Fig. 4. Schematic diagram of CPC1's readout.

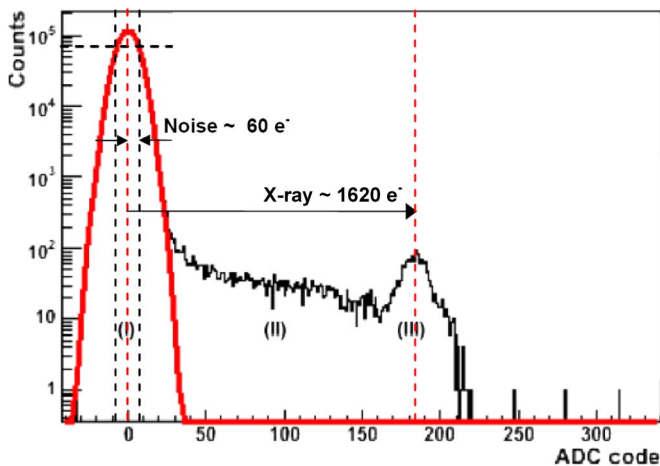


Fig. 5. Distribution of ADC codes for channel (column) two. Three regions are observed: (I) the high peak region which represents the noise, (II) the region separating the two peaks which represents the charge sharing between pixels, and (III) the X-ray peak region which represents the collected charge in a single pixel. The noise peak is fitted by a Gaussian function to determine the noise threshold. The standard deviation of the noise is about 60 electrons. The data was taken at $-80\text{ }^{\circ}\text{C}$ with 8 MHz readout frequency.

after the last pixel of the column. The average level of these is subtracted from all the pixels in the column.

As an example, Fig. 5 shows the pulse-height distribution for channel 2 summing up all reads in all the 400 pixels of the column. CTI is always calculated for channel 2 because it is physically adjacent to channels 1 and 3. This allows to apply a 3×3 cluster method (Fig. 6), in order to remove hits with charges from X-ray shared between pixels. This method is only applied to the 3 adjacent columns (1, 2 and 3). Column 2 is considered, where the signal charge of a pixel is accepted only if no charges from X-ray are present in the neighboring pixels.

The noise threshold is used to separate noise from charges shared between pixels. It is determined by fitting the noise peak with a Gaussian function. The threshold is usually set to be 5σ above the fitted peak centroid. Even after the 3-by-3 clustering,

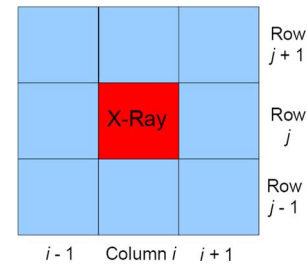


Fig. 6. Illustration of the 3×3 cluster method. A signal charge (from the X-ray) is only accepted if no charge from X-rays is present in the neighboring pixels. The X-ray charge is defined by its threshold determined after a first fit of the X-ray signal peak with a Gaussian function.

a tail remains (Fig. 7). In order to separate the X-ray signal region from the charge-sharing region we exclude all ADC codes below an X-ray threshold which is determined by fitting the X-ray peak. We set the threshold to be 2σ below the fitted peak centroid. In this way we obtain the measured X-ray signal data in the pixels with full X-ray charge (Fig. 8).

IV. BASELINE CORRECTION FOR DIFFERENT OPERATING TEMPERATURES AND READOUT FREQUENCIES

Owing to an RC coupling at the preamplifier input, the output voltage decays exponentially with a time constant equal to RC (τ_{RC} is of the order of $100\ \mu\text{s}$).¹ This is expected to give rise to an exponential baseline that varies during the clocking sequence, adding a contribution to the readout signal that depends on the pixel number. The shape of the baseline can be determined by comparing the average output level in the pixels to each other. For each pixel an average of the ADC codes was computed excluding the frames where the code exceeded the noise threshold. The average ADC code can usually be expected to be an exponential function of the pixel number with the RC decay. Figs. 9, 10, 11 and 12 show the distributions of the average ADC codes for all frames of a measurement as a function

¹For a readout frequency of 4 MHz reading out the whole column of 400 pixels takes a time comparable to τ_{RC} .

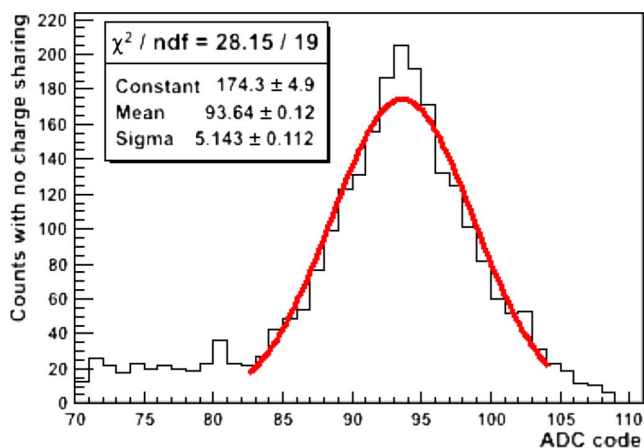


Fig. 7. X-ray signal peak with a tail from some charge sharing even after applying the 3×3 cluster method. The distribution is fitted with a Gaussian function to determine the threshold to be used to completely remove the charge sharing. This is a different dataset than that in Fig. 5, which was obtained using a higher preamplifier gain.

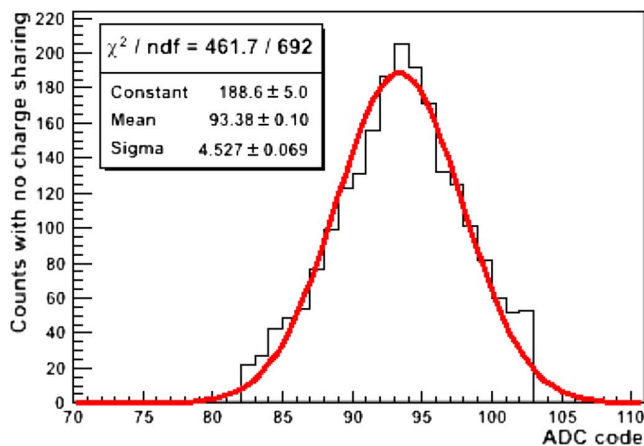


Fig. 8. X-ray peak after the removal of charge sharing.

of the pixel number for different readout frequencies and operating temperatures. These distributions are fitted by an exponential function given by $A \exp(-Bj)$, where A corresponds to the signal charge at the first pixel, B is the slope and j is the pixel number. This function will be subtracted from the X-ray data. Figs. 9 and 12 show approximately zero baseline level, whereas Figs. 10 and 11 show non-zero baseline fits. The baseline level is much smaller at low temperatures, for example at -60°C (Fig. 9) and at -109°C (Fig. 12). Figs. 10 and 11 show baselines for higher temperatures -6°C and -17°C , respectively. These observed baselines show different frequency dependence from what is expected from the RC effect. This indicates that other electronic effects also influence the baseline. For the same readout frequency (8 MHz) Figs. 11 and 12 show the temperature dependence explicitly.

V. DETERMINATION OF CHARGE TRANSFER INEFFICIENCY

The charge transfer inefficiency (CTI) in one pixel is defined as the ratio of signal lost during transfer (captured by traps) to the initial signal charge. In order to determine the CTI we first make the overclock correction and apply the 3×3 cluster method. Then, the X-ray peak was fitted with the Gaussian function to determine the X-ray threshold. This was used to construct

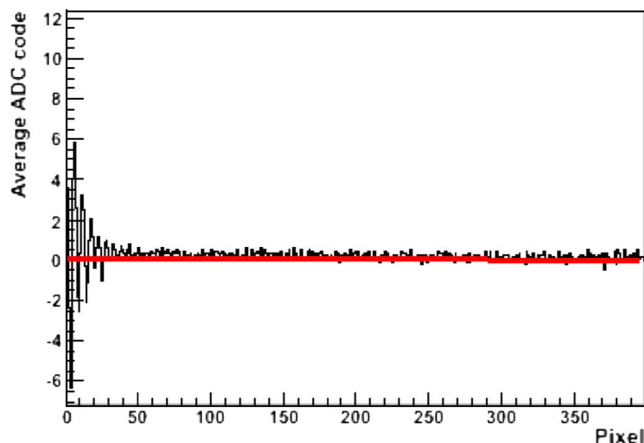


Fig. 9. Distribution of average ADC code in the noise region versus the pixel number at 2 MHz and -60°C with an exponential fit. The noise region was delimited by a 3σ noise threshold. Fit: amplitude $A = 0.117 \pm 0.056$ and exponent $B = (-5.29 \pm 2.85) \times 10^{-3}$.

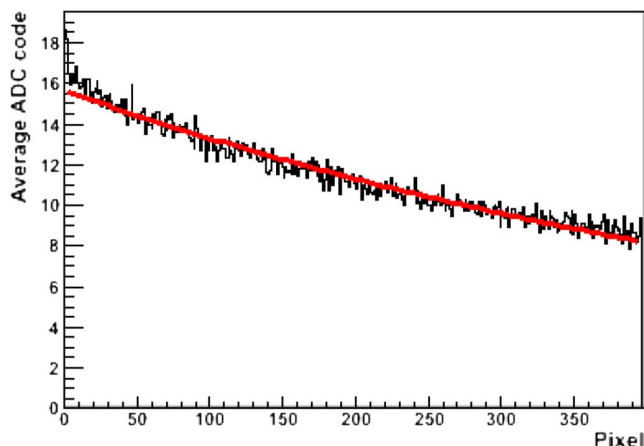


Fig. 10. Distribution of average ADC code in the noise region versus the pixel number at 4 MHz and -6°C with an exponential fit. The noise region was delimited by a 3σ noise threshold. Fit: amplitude $A = 15.64 \pm 0.44$ and exponent $B = (-16.24 \pm 1.33) \times 10^{-4}$.

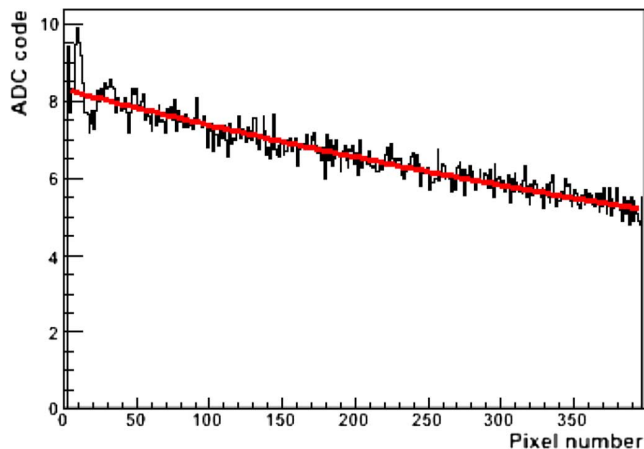


Fig. 11. Distribution of average ADC code in the noise region versus the pixel number at 8 MHz and -17°C with an exponential fit. The noise region was delimited by a 3σ noise threshold. Fit: amplitude $A = 8.31 \pm 0.31$ and exponent $B = (-11.86 \pm 1.74) \times 10^{-4}$.

the distribution with a fit of average ADC codes as shown in Fig. 13. The distribution is fitted with the first-order polynomial function $P_0 + P_1j$, where P_0 corresponds to the charge at the

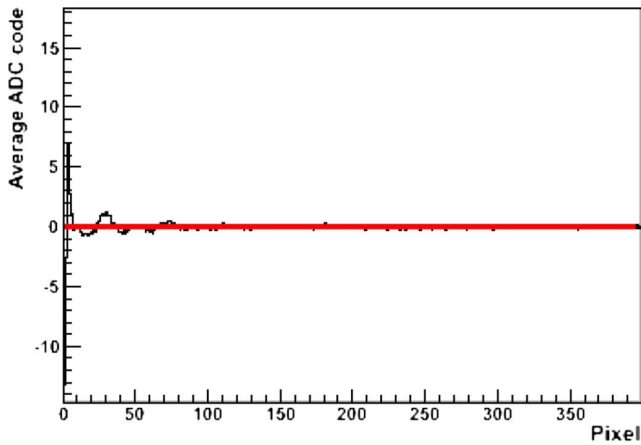


Fig. 12. Distribution of average ADC code in the noise region versus the pixel number at 8 MHz and -109°C with an exponential fit. The noise region was delimited by a 3σ noise threshold. Fit: amplitude $A = (0.082 \pm 5.035) \times 10^{-3}$ and exponent $B = (1.073 \pm 16.853) \times 10^{-2}$.

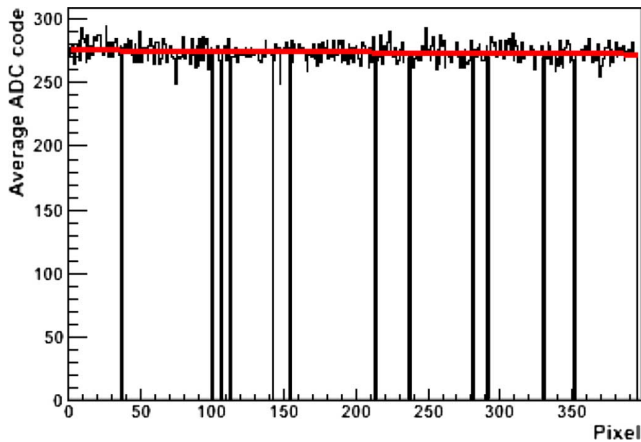


Fig. 13. Fit to average ADC codes without baseline removal at 2 MHz and -31°C . $CTI = (2.99 \pm 2.69) \times 10^{-5}$.

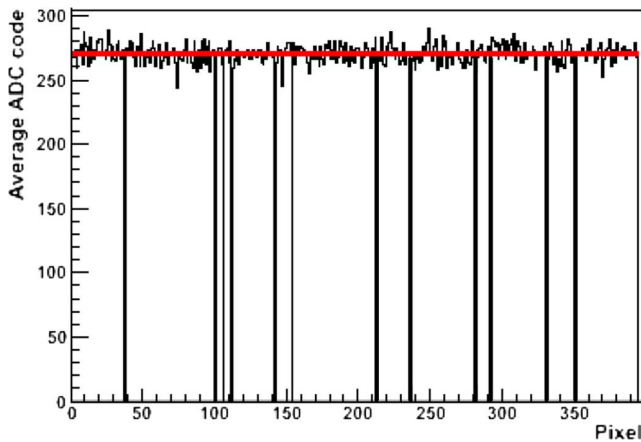


Fig. 14. Fit to average ADC codes with baseline removal at 2 MHz and -31°C . $CTI = (-0.09 \pm 2.70) \times 10^{-5}$.

first pixel, P_1 is the slope and j is the pixel number. This distribution is plotted without baseline removal. Fig. 14 shows the distribution of the averages as a function of pixel number with baseline removal. The CTI is determined for the two cases using $CTI = -P_1/P_0$.

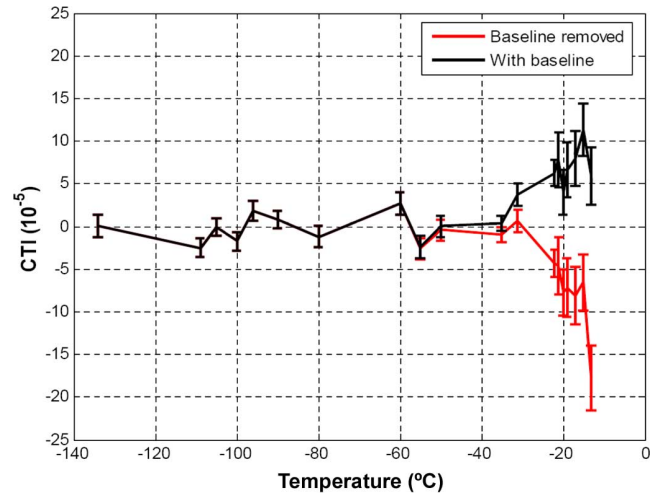


Fig. 15. CTI versus temperature at 2 MHz readout frequency. The CTI is shown resulting from fits to average ADC codes, with and without baseline removal. The shown error bars result from the precision of the fits.

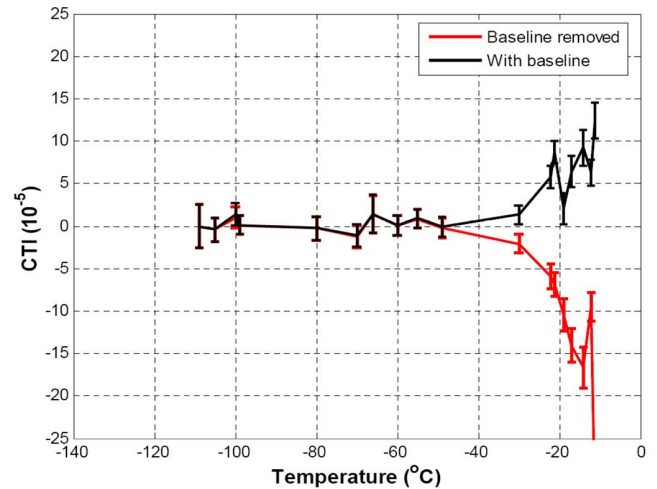


Fig. 16. CTI versus temperature at 4 MHz readout frequency. The CTI is shown resulting from fits to average ADC codes, with and without baseline removal. The shown error bars result from the precision of the fits.

VI. CTI RESULTS PRE-IRRADIATION FOR DIFFERENT READOUT FREQUENCIES

Figs. 15, 16 and 17 show the CTI values as a function of temperature for an un-irradiated CPC1 at different readout frequencies. The CTI has been calculated using a linear fit of average ADC codes versus pixel number. For this CCD with 400 pixels a CTI value of 10^{-5} means that only 0.4% of signal charge is lost, which is acceptable in normal operation. In the temperature region below -25°C no frequency dependence of the CTI measurements is observed. One may note that in the region of rather high temperatures (above -25°C) the effect of baseline removal is large and the determined CTI values indicate that the baseline effect is overestimated. The effect of the baseline removal decreases with increasing frequency as the readout clocking sequence becomes shorter compared to τ_{RC} (as visible in Fig. 17 for 8 MHz readout frequency).

The apparent trend of the CTI at high temperatures in the operating range used is probably due to the increase in background charge level as it is related to the dark current. The negative CTI

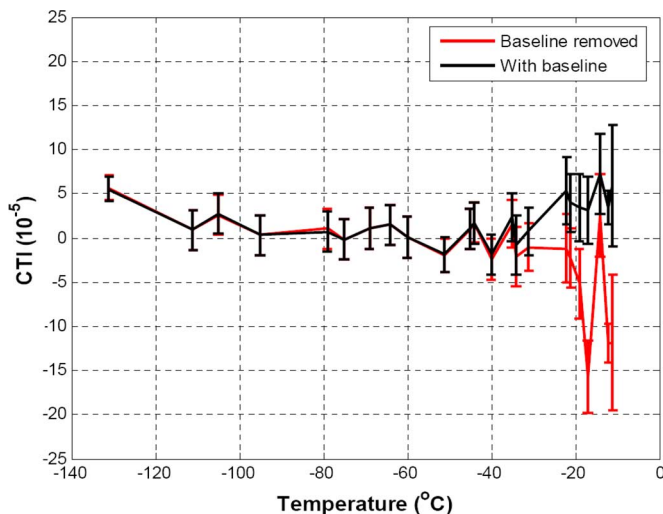


Fig. 17. CTI versus temperature at 8 MHz readout frequency. The CTI is shown resulting from fits to average ADC codes, with and without baseline removal. The shown error bars result from the precision of the fits.

is due to the difficulty in determining the baseline. The baseline is affected by the RC effect that decreases with the pixel number and the dark current that increases at high temperatures. This uncertainty in determining the baseline, which is subtracted from the X-ray peak, gives a negative value especially at high temperatures when the noise is high and closer to the X-ray peak. Also the low X-ray hit rate leads to a weak X-ray peak which leads to a bad fit and hence an additional uncertainty in the X-ray centroid determination. The accuracy of CTI calculation can be improved by putting the ^{55}Fe source in a position that it hits uniformly the CCD, carefully choosing the gain to use the ADC in its maximum dynamic and acquiring data in a large number of frames. A few measurements where a fraction of the data was lost in the sampling have been discarded.

VII. CONCLUSIONS AND OUTLOOK

An un-irradiated CPCCD is operated in a range of temperatures from $-10\text{ }^{\circ}\text{C}$ to $-136\text{ }^{\circ}\text{C}$ (liquid nitrogen cooling) with different readout frequencies 2, 4 and 8 MHz. The spectrum of a ^{55}Fe source is measured with this device. The CTI is analysed for different readout frequencies and operating temperatures. A clear X-ray signal is extracted by identifying isolated hits (3×3 method). The baseline is subtracted. The CTI value is small and compatible to the order of magnitude that can be expected for an un-irradiated CPCCD. Further CTI measurements with a CPCCD after irradiation and refinement of the analysis method are planned.

ACKNOWLEDGMENT

The authors would like to thank S. Aoulmit, C. Bowdery, A. Chilingarov, L. Dehimi, and N. Sengouga for discussions and comments on the manuscript. This work was supported by the Science and Technology Facilities Council (STFC) and Lancaster University. K. Bekhouche would like to thank the Algerian Government for financial support and Lancaster University for their hospitality. A. Sopczak would like to thank the Faculty of Science and Technology at Lancaster University for financial

support and the organizers of the IEEE 2008 conference for their hospitality.

REFERENCES

- [1] C. J. S. Damerell, "Radiation damage in CCDs used as particle detectors," *ICFA Instrum. Bull.*, vol. 14, p. 1, 1997.
- [2] K. Stefanov, "Radiation Damage Effects in CCD Sensors for Tracking Applications in High Energy Physics," Ph.D. dissertation, Saga Univ., Saga, Japan, 2001, and references therein; K. Stefanov, *et al.*, "Electron and neutron radiation damage effects on a two phase CCD," *IEEE Trans. Nucl. Sci.*, vol. 47, p. 1280, 2000.
- [3] LCFI Collaboration Homepage [Online]. Available: <http://hepwww.rl.ac.uk/lcfi/>
- [4] S. D. Worm, "Recent CCD development for the vertex detector of the ILC—Including ISIS (in-situ storage information sensors)," presented at the 10th Topical Seminar on Innovative Particle and Radiation Detectors. Siena, Italy, Oct. 1–5, 2006.
- [5] T. J. Greenshaw, "Column parallel CCDs and in-situ storage image sensors for the vertex detector of the international linear collider," in *Nuclear Science Symp.*, San Diego, CA, Oct. 29–Nov. 4 2006.
- [6] M. S. Robbins, "The Radiation Damage Performance of Marconi CCDs," Marconi Tech. Note S&C 906/424 2000 (unpublished).
- [7] J. E. Brau and N. B. Sinev, "Operation of a CCD particle detector in the presence of bulk neutron damage," *IEEE Trans. Nucl. Sci.*, vol. 47, p. 1898, 2000.
- [8] J. E. Brau, O. Igonkina, C. T. Potter, and N. B. Sinev, "Investigation of radiation damage in the SLD CCD vertex detector," *IEEE Trans. Nucl. Sci.*, vol. 51, p. 1742, 2004.
- [9] J. E. Brau, O. Igonkina, C. T. Potter, and N. B. Sinev, "Investigation of radiation damage effects in neutron irradiated CCD," *Nucl. Instrum. Meth. A*, vol. 549, p. 117, 2005.
- [10] J. E. Brau, O. Igonkina, N. B. Sinev, and J. Strube, "Investigations into properties of charge traps created in CCDs by neutron and electron irradiation," *Pramana-J. Phys.*, vol. 69, p. 1093, 2007.
- [11] A. M. Mohsen and M. F. Tompsett, "The effect of bulk traps on the performance of bulk channel charge-coupled devices," *IEEE Trans. Electron Dev.*, vol. ED-11, p. 701, 1974.
- [12] I. H. Hopkins, G. Hopkinson, and B. Johlander, "Proton-induced charge transfer degradation in CCD's for near-room temperature applications," *IEEE Trans. Nucl. Sci.*, vol. 41, p. 1984, 1994.
- [13] T. Hardy, R. Murowinski, and M. J. Deen, "Charge transfer efficiency in proton damaged CCD's," *IEEE Trans. Nucl. Sci.*, vol. 45, p. 154, 1998.
- [14] A. Sopczak, "LCFI charge transfer inefficiency studies for CCD vertex detectors," in *Proc. IEEE Nuclear Science Symp.*, San Juan, PR, 2005, p. 1494, IEEE Nuclear Science Symp. Conf. Record N37-7.
- [15] A. Sopczak, "Radiation hardness of CCD vertex detectors for the ILC," in *Proc. IEEE Nuclear Science Symp.*, San Diego, CA, Oct. 29–Nov. 4 2006, p. 576, IEEE Nuclear Science Conf. Record N14-215 (2006).
- [16] A. Sopczak *et al.*, "Simulations of the temperature dependence of the charge transfer inefficiency in a high-speed CCD," *IEEE Trans. Nucl. Sci.*, vol. 54, p. 429, 2007, and references therein.
- [17] A. Sopczak *et al.*, "Radiation hardness studies in a CCD with high-speed column parallel readout," in *Proc. IEEE Nuclear Science Symp.*, Honolulu, HI, Oct. 27–Nov. 3 2007, p. 2278, IEEE Nuclear Science Conf. Record N48-2 (2007).
- [18] A. Sopczak *et al.*, "Radiation hardness studies in a CCD with high-speed column parallel readout," *JINST*, vol. 3, p. 5007, 2008.
- [19] T. Maruyama, *Private Communication*. 2006, Stanford (Linear Accelerator Center, SLAC).
- [20] A. Vogel, *Private Communication*. 2006, (DESY Hamburg).
- [21] J. W. Walker and C. T. Sah, "Properties of 1.0-MeV-electron-irradiated defect centers in silicon," *Phys. Rev.*, vol. B7, p. 4587, 1972.
- [22] N. S. Saks, "Investigation of bulk electron traps created by fast neutron irradiation in a buried n-channel CCD," *IEEE Trans. Nucl. Sci.*, vol. NS-24, p. 2153, 1977.
- [23] J. R. Srouf, R. A. Hartmann, and S. Othmer, "Transient and permanent effects of neutron bombardment on a commercially available N-buried-channel CCD," *IEEE Trans. Nucl. Sci.*, vol. NS-27, p. 1402, 1980.
- [24] R. M. Ambrosi *et al.*, "The impact of low energy proton damage on the operational characteristics of EPIC-MOS CCDs," *Nucl. Instrum. Meth. B*, vol. 207, p. 175, 2003.
- [25] A. F. Abbey *et al.*, "Cooling out the radiation damage on the XMM-Newton EPIC MOS CCDs," *Nucl. Instrum. Meth. A*, vol. 513, p. 136, 2003.
- [26] ROOT Homepage [Online]. Available: <http://root.cern.ch/>